

## RESEARCH ARTICLE

# Design and Implementation of a Single Switch High Gain Boost Topology: Structure, Ripple Control and ZCS

MOHAMMAD FARSIJANI<sup>1</sup>, (Member, IEEE), SOHRAB ABBASIAN<sup>1</sup>, (Member, IEEE),  
HOSSEIN HAFEZI<sup>2</sup>, (Senior Member, IEEE),  
MOHAMMAD TAVAKOLI BINA<sup>1</sup>, (Senior Member, IEEE),  
AND KARIM ABBASZADEH<sup>1</sup>

<sup>1</sup>Faculty of Electrical Engineering, K. N. Toosi University of Technology, Tehran 19697, Iran

<sup>2</sup>Faculty of Information Technology and Communications, Tampere University, 33100 Tampere, Finland

Corresponding author: Hossein Hafezi (hossein.hafezi@tuni.fi)

**ABSTRACT** The need for high gain DC-DC converters has lately increased in tandem with the utilization of renewable energy supplies. Particularly appealing are high gain converters that do not require the inclusion of extra power switches and/or other passive elements to the system. As a result, this study proposes a non-isolated single switch converter with ultra-high voltage gain (UHG) that is appropriate for most renewable energy conversion systems, like solar installations. With only a single MOSFET working within a suitable duty cycle region, the proposed converter provides significant voltage gain and around 95% efficiency. Moreover, the MOSFET in this UHG converter is turned on in zero current switching (ZCS) mode, resolving the diode recovery issue. The recommended UHG converter's working modes, steady-state parametric study, circuit variables like voltage stress on switching devices, and converter gain are all thoroughly explained. Comparisons have been done with comparable topologies presented in the literature, and lastly, experimental results depending on 200W (20V input, 320V output voltage) are given to validate the operation of the proposed UHG design.

**INDEX TERMS** Ultra high gain converter, DC-DC topology, three-windings coupled-inductor, soft switching, zero current switching, high gain step-up converter.

## I. INTRODUCTION

In past years, there has been a significant growth in energy demand and usage. This expansion is projected to continue over the next many years (at least). Conventional fossil-fueled sources of energy are linked to two fundamental issues: finite resources and greenhouse gas emissions. As a result of these worries, companies have invested in environmentally acceptable energy resources such as photovoltaic (PV) devices [1], [2], hydrogen-based fuel cells [3], [4], and wind energy technologies.

In the majority of these novel energy methods, the produced power is either direct current (DC) or there is an intermediary DC connection in the energy conversion system [5].

The associate editor coordinating the review of this manuscript and approving it for publication was Kan Liu<sup>1</sup>.

Solar panels, as a standard strategy for PV systems, can be arranged in parallel or in series with one another and operate as the input for DC-DC topologies, the primary tasks of those are to control and step up the DC voltage on the DC-link for DC-AC conversion. In order to control the current rating of the switching devices and utilize the suitable modulation coefficients, the DC-link voltage of a DC-AC inverter must not be less than a particular specified value. In past research, several designs were created to increase the voltage level of PV panels to an acceptable amount for the DC-link voltage.

Combining coupled inductor (CI) and passive and active clamped approaches, high boosting capability can be accomplished [6], [18]. Despite these, the cost and dimensions of this converter, due to its two output DC-link capacitors and CI's enormous core size, do not appear to be appropriate for the entire power rating.

Further approaches for achieving high voltage gain in switching mode converters include the use of a switched capacitor or a switched inductor [7], [15]. However, due to the intrinsic characteristic of these designs [7], [14], a high duty cycle value is required for active switch(es) to accomplish high voltage gain in several high gain step-up converters, that might raise switching losses. The active switched-inductor with a passive switched-capacitor based converter described in [24] increased voltage gain via a cascaded passive switched-capacitor network. But, the inductance in the high-side LC filter, that is utilized to minimize the discharge current spikes of capacitors, will result in a bulkier circuit based on the calculated inductance. The voltage gain of an active switched inductor converter is improved in [25] by using an extensive active-passive inductor unit. By expanding the amount of active-passive inductance cells, voltage stress on switches is diminished and critical inductance is lowered, but the semiconductor device drive circuit becomes more complicated due to the extra switches. Reference [8] introduces a unique resonant design with a double voltage arrangement and two sets of secondary windings to produce soft switching operation. The disadvantage of this converter is that it has a high number of active switching devices as compared to single-switch designs.

Another typical approach for improving voltage gain in DC-DC converters is to change the turn-ratio of specific magnetic elements, such as a transformer or CI [9], [12], [13], [14], [15]. In particular applications when isolation is not required, the CI is used by varying the turns ratio, that can yield significant voltage gain. Compared with an isolation transformer, the coupled inductor has a simple and efficient structure, but its use is restricted to applications that do not require electrical isolation [28], [29]. Considering its adaptability, the high voltage gain method has significant drawbacks, the majority of which are related to CI leakage [10], [11]. Using multiplier cells in a boost converter is another way to enhance voltage gain [16], [18], [20], [24]. The turns ratio of the CI is the most critical factor in increasing voltage gain and reducing voltage stress over the switches. The DC-DC design in [15] operates well in terms of voltage gain and voltage stress. But at the other hand, the current ripple is significantly larger on the input-voltage side. As a result, the power source's lifetime may be diminished, as well as its overall efficiency.

In [17], the researchers suggested a novel DC-DC converter design depending on 3 CI with high voltage gain. While the use of inexpensive elements with CI is a benefit of this design, the voltage gain is too low to be employed for a DC-DC-AC solar systems with a specific solar panel. Another three-winding CI-based converter has been suggested in [13], but it suffers from reverse-recovery issues due to their diodes. Reference [22] proposes a new configuration for a step-up DC-DC converter with a high voltage transfer gain and an appropriate duty cycle. However, due to the use of resistance in the power input path, the ripple of input current is higher than that of other step-up topologies, such as those described

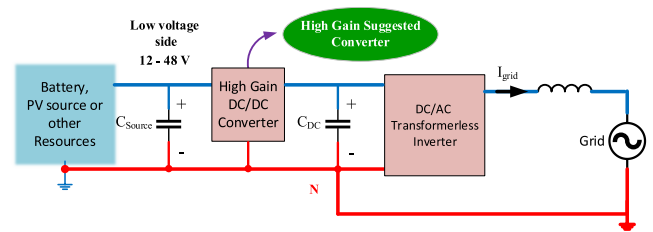


FIGURE 1. An example application of proposed converter.

in [19], [20], and [21], and the efficiency can be reduced. In addition, the diode voltage stress in the multiplier cell of this converter is equal to the output diode voltage, which can increase the overall price of the converter.

A non-isolated ultra-high gain (UHG) DC-DC configuration with three winding CI and a single power MOSFET switch is presented in this work. The main features of the proposed converter are:

- Very low Input current ripple.
- Low voltage Stress on semiconductors.
- High and appropriate voltage gain of the converter.
- Soft switching operation for main switch and diodes.
- Appropriate total efficiency of converter.

Fig. 1 shows an example application of proposed converter in a grid integration of energy resource. It should be noted that in grounded PV systems, the step-up converter should provide a shared ground between the PV ground and the grid neutral line to prevent common mode current. That's why there is a common input to output ground in the proposed topology.

The proposed converter can be used in PV applications under normal or partial shading conditions as well as other applications such as Fuel cells, DC microgrid and HID lamp ballast. For example, when partial shading occurs on a solar system, the maximum power point of that system may be formed at low voltage levels. Therefore, it is necessary to use a high gain step-up converter.

This work extends the proposed UHG converter topology which was previously presented at a conference [24], where more detail analysis has been done on device operation, evaluation of the current stress on semiconductor devices have been done, comparative study is extended, the component design procedure of the proposed converter has been explained and followed by numerical representation in the experimental setup development. Moreover, more detail efficiency analysis and losses evaluation have been performed to compare the proposed converter efficiency with most recent similar topologies available in the literature.

It is important to note that adding voltage gain using a large number of inductors will not happen easily, and significant challenges such as voltage stress on the switch(es) or diodes, Soft/Hard switching operation, losses of windings should be considered.

The remaining of this paper is organized as follows: Section II discusses circuit designing and operational analysis in the context of continuous conduction mode (CCM).

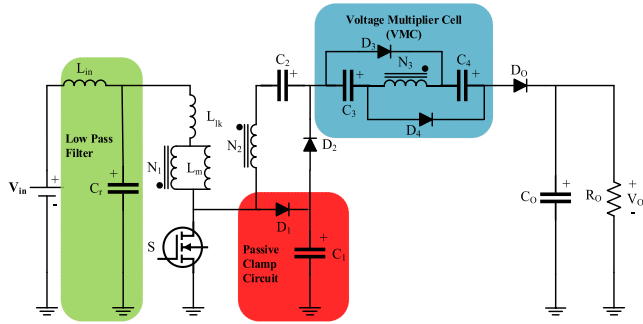


FIGURE 2. Suggested UHG DC-DC topology.

Section III obtains some critical topology characteristics (including voltage gain and voltage stress over the switching devices). There is the component design and efficiency analysis in Section IV. Section V includes a comparison between comparable high gain designs available in the literature. Lastly, Section VI discusses the paper’s overall accomplishments depending on the experimental setup. While the closed-loop control can be achieved for different purposes (e.g. output voltage regulation using a conventional PI), this research concentrates on the design of the high gain boost converter along with the soft switching circuit assignment as well as low-ripple input current regulation.

II. SUGGESTED TOPOLOGY AND OPERATION PRINCIPLES

The suggested design comprises a voltage multiplier cell (VMC) and a CI to improve converter boosting capabilities. Figure 2 depicts the suggested UHG DC-DC converter associated power circuit. A passive clamping circuit consists of capacitor C1 and diode D1 is employed to relieve the voltage spike caused by the leakage inductor on the main MOSFET and recycle the leakage inductance energy. To improve the converter voltage gain, at the tertiary side of the CI, capacitors C3 and C4, and diodes D3 and D4 work as a VMC. The LC low-pass filter at the input makes the input current continuous with low ripple, which makes the proposed converter suitable for use in renewable sources such as solar cells.

The condition of switching devices in one entire switching period for the proposed UHG DC-DC converter is depicted in Fig. 3, wherein a switching period is split into six subintervals (mode 1 - mode 6). Figure 4 depicts the primary waveforms of currents and voltages during a single switching period. The following concepts are taken into account when performing the steady-state analysis:

- The switch and other semiconductors are ideal.
- CI is considered ideal with the turns-ratio of  $n_2 = N_2/N_1$ ,  $n_3 = N_3/N_1$ , magnetizing inductor ( $L_m$ ) and leakage inductor ( $L_{lk}$ ).
- The grayed-out components are disabled.
- The suggested topology (Fig.2) works in (CCM).
- D denotes duty cycle of the switch and D’ is equal to 1-D.

The following are the suggested design operating principles:

**Mode 1:** At the commencement of the first state, the MOSFET starts to conduct, diodes  $D_1 - D_4$  are blocked, and only  $D_0$  is conducting. As the leakage inductance current,  $I_{lk}$ , slowly rises during this small time, the currents on the different sides of the CI ( $I_{N2}$  and  $I_{N3}$ ) reduce gradually. According to Fig. 3(a), the existence of  $L_{in}$  and a leaky inductor causes MOSFET current to progressively rise and turning on in a ZCS condition. Whenever the leakage current reaches the magnetizing current, diode  $D_0$  switches off and diode  $D_2$  turns on.

**Mode 2:** In Fig. 3(b), the MOSFET remains operating in the second mode, and diodes  $D_3, D_4,$  and  $D_0$  are blocked, whereas diode  $D_2$  is turned on with a ZCS condition. The input, leakage, and magnetizing inductors are charged by the DC input voltage source, increasing their current ( $I_{Lin}, I_{Lm},$  and  $I_{Lk}$ ). The diode  $D_2$  discharges the capacitor  $C_1$  and charges the capacitor  $C_2$ .

These formulae can be determined by applying Kirchoff’s Voltage Law (KVL) to the design in this mode:

$$V_{Lm}^D = \left[ \frac{L_m}{L_m + L_{lk}} \right] V_{Cr} = kV_{Cr} \tag{1}$$

$$V_{Llk}^D = \left[ \frac{L_{lk}}{L_m + L_{lk}} \right] V_{Cr} = (1 - k)V_{Cr} \tag{2}$$

$$V_{Lin}^D + V_{Lm}^D + V_{Llk}^D = V_{in} \tag{3}$$

$$V_{Lin}^D + V_{Cr} = V_{in} \tag{4}$$

$$V_{N2}^D = V_{C2} - V_{C1} = n_2 V_{Lm}^D = n_2 k V_{Cr} \tag{5}$$

k is the coupling factor and  $V_{Lm}^D, V_{Llk}^D, V_{Lin}^D$  are voltage of magnetizing, leakage and input inductances while MOSFET is on respectively.  $V_{Cr}, V_{C2}, V_{C1}$  are voltage of capacitors  $C_r, C_2$  and  $C_1$  respectively, while MOSFET is turned on. This interval ends when the diodes  $D_3$  and  $D_4$  turn on and amplitude of  $I_{N3}$  increases.

**Mode 3:** In this state, the MOSFET stays switched on, and diodes  $D_2, D_3$  and  $D_4$  conduct while diodes  $D_1$  and  $D_0$  are turned off. Through the diode  $D_2$ , the capacitor  $C_1$  is discharged, while the capacitors  $C_3, C_4,$  and  $C_2$  are charged. Furthermore, because of the inverted voltage on windings  $N_3$  and  $N_2$ , the currents on windings  $N_2$  and  $N_3$  ( $I_{N2}$  and  $I_{N3}$ ) are gradually decreasing. Moreover, the voltages of capacitors  $C_3$  and  $C_4$  are determined in this situation using (6):

$$V_{N3}^D = V_{C3} = V_{C4} = n_3 V_{Lm}^D = n_3 k V_{Cr} \tag{6}$$

where  $V_{N3}^D$  is the voltage of tertiary windings whenever the MOSFET is on.

**Mode 4:** This short interval transition starts whenever currents of windings  $N_2$  and  $N_3$  is near zero and all diodes are blocked. As it can be found from Fig. 4, while the switch is completely off, this time interval ends.

**Mode 5:** In this situation, the power switch is switched off, and the input voltage charges the windings of  $N_2$  and  $N_3$ . The energy from the leaking inductor is recycled to the capacitor  $C_1$ , which is supplied through the diode  $D_1$ . For

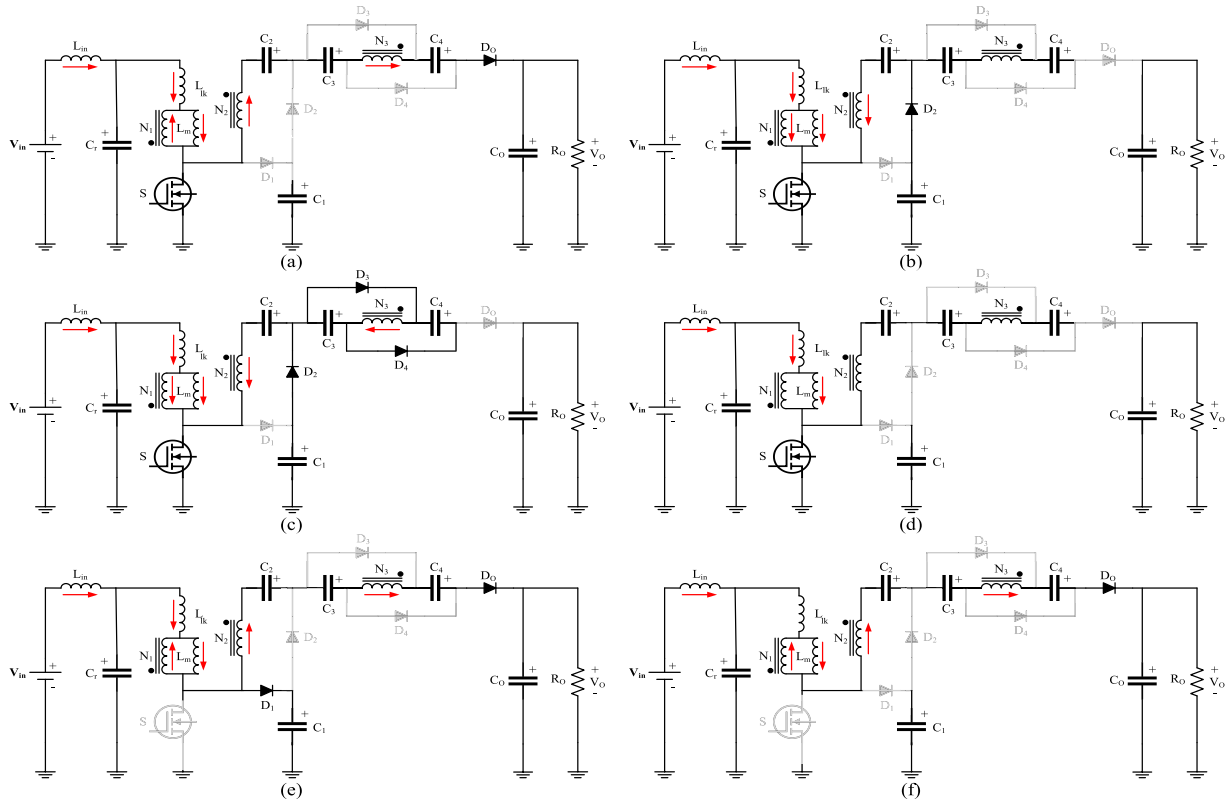


**FIGURE 3.** Current paths in the suggested UHG topology, (a) circuit status at Mode 1, (b) circuit status at Mode 2, (c) circuit status at Mode 3, (d) circuit status at Mode 4, (e) circuit status at Mode 5, (f) circuit status at Mode 6.

now, capacitors C2, C3, and C4 are discharged via the output diode. The following formula can be obtained by considering KVL in the loop of Fig. 3(e):

$$V_{Lm}^{D'} + V_{Lm}^{D'} + V_{Llk}^{D'} = V_{in} - V_{C1} \quad (7)$$

$$V_{Lm}^{D'} = k(V_{Cr} - V_{C1}) \quad (8)$$

$$V_{N2}^{D'} = n_2 V_{Lm}^{D'} \quad (9)$$

$$V_{N3}^{D'} = n_3 V_{Lm}^{D'} \quad (10)$$

$$V_{C1} - V_{N2}^{D'} + V_{C2} + V_{C3} - V_{N3}^{D'} + V_{C4} = V_O \quad (11)$$

where  $V_{Lm}^{D'}$ ,  $V_{Llk}^{D'}$ ,  $V_{Lm}^{D'}$  are voltage of magnetizing, leakage and input inductances while the MOSFET is off respectively.

**Mode 6:** The power switch is continuously blocked in this situation, and this state starts whenever the voltage of C1 approaches its ultimate amount and D1 goes off. As in the preceding state, capacitors C2, C3 and C4 are discharged through the output diode in this mode (D0). Whenever the MOSFET is switched on, Mode 6 comes to an end, and the next cycle begins.

### III. STEADY-STATE ANALYSIS OF THE SUGGESTED DESIGN

#### A. VOLTAGE GAIN ( $M_{CCM}$ ) CALCULATION

By utilizing the volt-second equilibrium axiom for both input inductor and magnetizing inductance, using (3) and (7),  $V_{C1}$

can be related to input voltage by:

$$V_{C1} = \frac{V_{in}}{D'} \quad (12)$$

According to (12) and by utilizing the volt-second equilibrium axiom for magnetizing inductance, using (1) and (8),  $V_{Cr}$  is obtained by:

$$V_{Cr} = D' V_{C1} = V_{in} \quad (13)$$

By substituting (12) and (13) into (5) the  $V_{C2}$  is obtained:

$$V_{C2} = n_2 k V_{in} + \frac{V_{in}}{D'} \quad (14)$$

By substituting (12) and (13) into (8) the  $V_{Lm}^{D'}$  relation to input voltage can be obtained by:

$$V_{Lm}^{D'} = k(V_{Cr} - V_{C1}) = -\frac{D}{D'} V_{in} \quad (15)$$

By substituting (6), (9), (10), (12), (13), (14), and (15) into (11) the nominal  $M_{CCM}$  of proposed UHG topology is obtained:

$$\frac{V_o}{V_{in}} = \frac{1}{D'} (2 + n_2 (D + kD') + n_3 (D + 2kD')) \quad (16)$$

If the leakage inductance of the CI is not considered, the coupling factor k is 1, and the ideal  $M_{CCM}$  of the proposed topology is as follows:

$$M_{CCM} = \frac{V_o}{V_{in}} = \frac{1}{D'} (2 + n_2 + n_3 (D + 2D')) \quad (17)$$

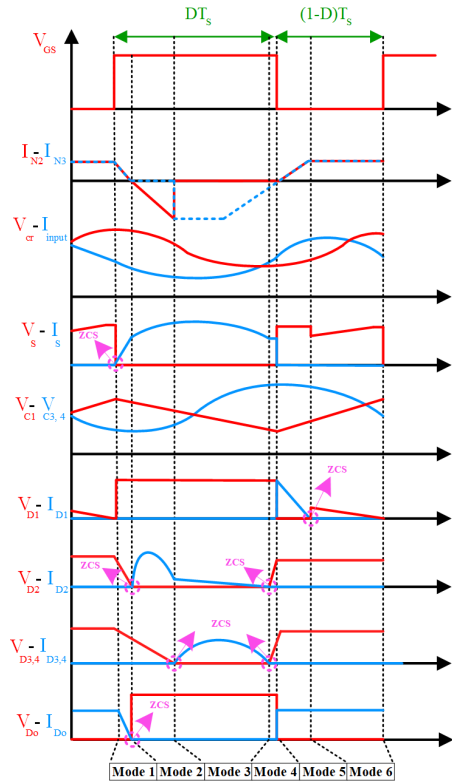


FIGURE 4. Essential waveforms of the suggested topology in CCM operation.

Figure 5(a) shows the voltage gain of the converter in the different secondary and tertiary turns ratio when duty cycle is 0.5. As it is clear in this picture, in addition to the high turns ratio, in the lower turns ratio, using the suggested converter, a suitable voltage gain can be obtained. The suggested topology theoretical voltage gain in CCM,  $M_{CCM}$ , versus MOSFET duty cycle,  $D$ , for different CI,  $n_2$  and  $n_3$  turn ratios is illustrated in Fig. 5. (b). It can be shown that the CI turns ratios,  $N_2$  and  $N_3$ , can be determined and changed to provide very high voltage gain without ever using and operating at an extremely high duty cycle.

Due to the significant increase in power switch conduction losses and the need for a larger heatsink at higher duty cycles, the appropriate duty cycle value of the MOSFET for this topology is less than 0.75, below the knee point of the curves shown in Fig. 5(b)

**B. EVALUATION OF VOLTAGE STRESS ON SEMICONDUCTOR DEVICES**

The voltage stress of switch and other semiconductors based on the topology operation are calculated as follows:

$$V_S = V_{D1} = V_{C1} = \frac{V_{in}}{D'} \tag{18}$$

$$V_{D2} = (n_2 + 1) \frac{V_{in}}{D'} \tag{19}$$

$$V_{D3} = V_{D4} = n_3 \frac{V_{in}}{D'} \tag{20}$$

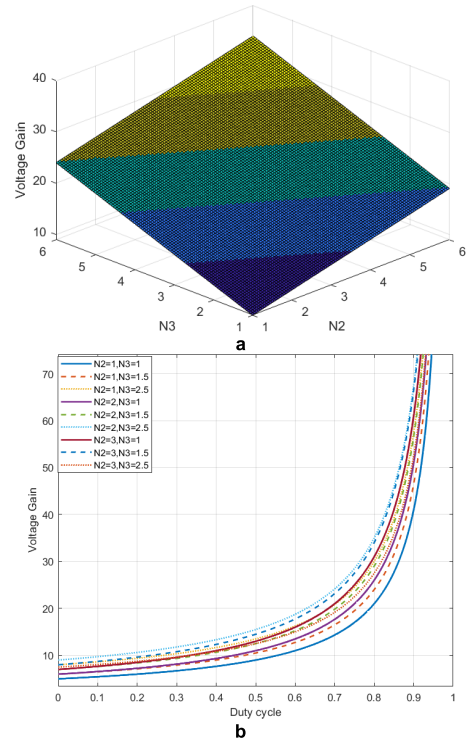


FIGURE 5. a) Voltage gain in different secondary and tertiary turns ratio ( $D = 0.5$ ), b)  $M_{CCM}$  against duty cycle under various CI turns ratios ( $N_1 = 1$ ).

$$V_{DO} = (1 + n_2 + n_3) \frac{V_{in}}{D'} \tag{21}$$

where,  $V_s$  is voltage stress on MOSFET and  $V_{D1}$ ,  $V_{D2}$ ,  $V_{D3}$  and  $V_{DO}$  are voltage stress of Diodes  $D_1$ ,  $D_2$ ,  $D_3$  and  $D_0$  respectively.

**C. EVALUATION OF CURRENT STRESS ON SEMICONDUCTOR DEVICES**

By using ampere-second balance law on all capacitors,  $C_1$ ,  $C_1-C_4$  and  $C_o$ , the average currents of all diodes are equal to the output current,  $I_o$ . Following the same procedure presented in [22], the peak current of the switch and diodes are calculated as follows:

$$I_{D1} = \frac{1}{D'}(1 + n_2 + n_3 (D + 2D'))I_o \tag{22}$$

$$I_{D2} = I_{D3} = I_{D4} = 2 \frac{I_o}{D} \tag{23}$$

$$I_{D0} = \frac{I_o}{D'} \tag{24}$$

$$I_S = \frac{1}{DD'}(1 + D(1 + n_2 + n_3 (D + 2D'))I_o + \frac{1}{2} \frac{V_{in}D}{L_m f_s} \tag{25}$$

Voltage and current stresses are important information for semiconductor devices selection.

Figures 6(a-c) show the normalized voltage stress on the diodes  $D_2$ ,  $D_3$  and  $D_0$  respectively when duty cycle is 0.5. Furthermore, the normalized current stress through the Diode



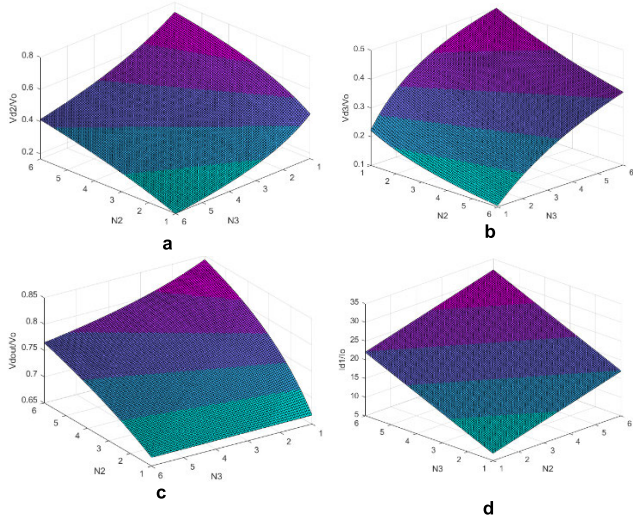


**FIGURE 6.** Normalized Voltage stress on: a)  $D_2$ , b)  $D_3$ , c)  $D_0$  in different secondary and tertiary turns ratio ( $D = 0.5$ ,  $N_1 = 1$ ), d) Normalized current stress of  $D_1$ .

$D_1$  is depicted in Fig. 6(d). By using these figures, the optimal values of turns ratio can be selected.

#### D. VOLTAGE AND CURRENT STRESS OF PASSIVE COMPONENTS

The voltage stress of passive components can be obtained using equations (6-10), (12-14), (17) as follows:

$$V_{C1} = \frac{V_{in}}{D'} \quad (26)$$

$$V_{C2} = (n_2 + \frac{1}{D'})V_{in} \quad (27)$$

$$V_{C3} = V_{C4} = n_3 V_{in} \quad (28)$$

$$V_{Co} = \frac{V_{in}}{D'}(2 + n_2 + n_3(D + 2D')) \quad (29)$$

$$V_{Lm} = (1 - \frac{1}{D'})V_{in} \quad (30)$$

$$V_{N2} = (1 - \frac{1}{D'})V_{in}n_2 \quad (31)$$

$$V_{N3} = (1 - \frac{1}{D'})V_{in}n_3 \quad (32)$$

Furthermore, the current stress of passive components can be obtained using operation modes and by assuming efficiency around to %100 for nominal output power. Besides that, the RMS current of  $C_r$  is very low.

$$RMS(i_{C1} = i_{C2} = i_{C3} = i_{C4}) \sim i_o \quad (33)$$

$$i_{Lin,rms} \sim \frac{1}{D'}(2 + n_2 + n_3(D + 2D'))i_o \quad (34)$$

$$i_{lm,rms} \sim \frac{1}{DD'}(1 + D(1 + n_2 + n_3(D + 2D'))I_O \quad (35)$$

## IV. COMPONENT DESIGN

### A. INPUT FILTER DESIGN (LIN)

By assuming the acceptable ripple on input inductance ( $\Delta I_{in}$ ), and knowing the switching frequency of the active switch ( $f_s$ ),

using (33), the size of input inductor can be obtained from the following equation:

$$L_{Lin} \geq \frac{V_{in}D}{\Delta I_{in}f_s} \quad (36)$$

### B. CAPACITORS DESIGN

The following equation is used to calculate the size of capacitors except resonance capacitor.

$$C \geq \frac{P_O}{V_C \Delta V_C f_s} \quad (37)$$

### C. COUPLED INDUCTOR MAGNETIZING INDUCTANCE DESIGN ( $L_m$ )

By assuming acceptable current ripple on coupled inductor magnetizing inductance ( $\Delta I_{Lm}$ ), the amount of the magnetic inductance can be obtained from the following equation:

$$L_m \geq \frac{V_{in}D}{\Delta I_{Lm}f_s} \quad (38)$$

Fig. 7 shows the boundary Region between DCM and CCM for different output power of suggested converter. Using  $L_m = 140 \mu\text{H}$  the suggested design operates for most output powers in the CCM.

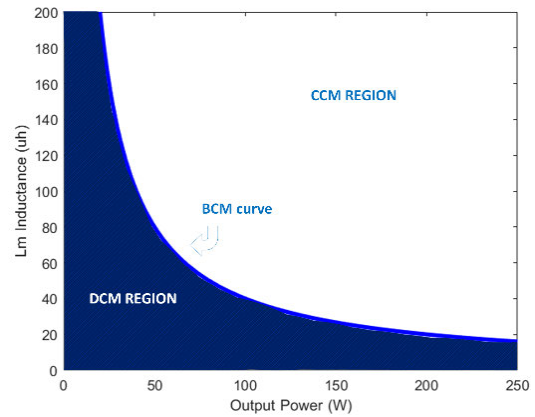


**FIGURE 7.** DCM and CCM region for different output power.

The average current of magnetic inductance ( $L_m$ ) is determined as follow:

$$I_{Lm} = I_{in} = \frac{1}{D'}(2 + n_2 + n_3(D + 2D'))I_O \quad (39)$$

### 1) DESIGN OF RESONANCE COMPONENTS

To calculate the amount of  $C_r$  (resonance capacitor) and coupled inductor leakage inductance ( $L_{lk}$ ), according to [22], these components are designed to operate in boundary-resonance or blow-resonance mode to reduce output diode switching losses and improve its reverse recovery problems. Also the amount of  $L_{lk}$  depends on how coupled inductor winding is wrapped and thus the following equation can be used for design purpose:

$$\pi \sqrt{L_{lk} C_r} \leq DT_s \rightarrow C_r \leq \frac{D^2}{\pi^2 L_{lk} f_s^2} \quad (40)$$

**TABLE 1.** Comparison of a proposed UHG DC-DC converter with some other high step-up topologies.

Converters	Ref [12], 2019	Ref [13], 2015	Ref [14], 2019	Ref [15], 2017	Ref [16], 2016	Ref [17], 2019	Ref [18], 2020	Ref [19], 2018	Ref [20], 2016	Ref [21], 2018	Proposed Converter
$N_c$	4	4	4	3	3	3	4	5	4	3	6
$N_s$	1	1	2	4	1	1	1	4	2	1	1
$N_D$	4	4	2	0	2	3	3	5	4	3	5
$N_{IND}$	1C(3W)	1C(3W)	1+1C(2W)	1C(2W)	1+1C(2W)	1C(3W)	1+1C(2W)	2C(2W)	1C(3W)	1C(3W)	1+1C(3W)
Common input to output Ground	✓	✓	✓	✓	✓	✓	✓	✓	✗	✓	✓
Efficiency & Voltage ratio	96% At(400W) 40V to 380V	95.2% At(200W) 90V to 400V	95.8% At(300W) 48V to 400V	94.8% At(200W) 25V to 200V	93.1% At(200W) 35V to 380V	94.2% At(200W) 20V to 300V	94.6% At(250W) 20V to 143V	95.7% At(150W) 72V to 400V	94.4% At(200W) 30-50V to	97.4% At(400W) 20V to 400V	95.8% At(200W) 17-20V to 320V
Input current ripple	Low	High	Very low	High	Very low	High	Low	High	High	High	Very low
Voltage Stress on output diode	$\frac{(n_3)V_o}{(1-D)(n_2-1)}$	$\frac{(n_2+1)V_o}{n_3+n_2+2-(1+n_2)D}$	$V_o$	$\frac{n_2}{2n_2-1}V_o$	$V_o$	$\frac{(n_2+n_3)V_o}{n_2+n_3+D(n_3-1)}$	$\frac{n_2V_o}{2n_2-1}$	$V_o$	$\frac{n_3 \cdot V_o}{n_3+1+D}$	$\frac{n_2+n_3}{2n_2+n_3-1}V_o$	$\frac{(n_2+n_3+1)V_o}{n_2+n_3(2-D)+2}$
Voltage Stress on main switch	$\frac{(n_2-1)V_o}{n_3+2n_2-1}$	$\frac{V_o}{n_3+n_2+2-(1+n_2)D}$	$\frac{V_o}{n_2}$	$2V_o$	$\frac{V_o}{n_2+1}$	$\frac{(n_3-1)V_o}{n_2+n_3+D(n_3-1)}$	$\frac{(n_2-1)V_o}{2n_2-1}$	$\frac{V_o}{1+n_2}$	$\frac{V_o}{1+n_3+D}$	$\frac{n_2-1}{2n_2+n_3-1}V_o$	$\frac{V_o}{2+n_2+n_3(2-D)}$
Voltage Gain	$\frac{n_3+2n_2-1}{(1-D)(n_2-1)}$	$\frac{n_3+2-D+n_2(1-D)}{1-D}$	$\frac{n_2}{1-D}$	$\frac{2n_2-1}{(n_2-1)(1-D)}$	$\frac{n_2+1}{1-D}$	$\frac{n_2+n_3+D(n_3-1)}{(n_3-1)(1-D)}$	$\frac{2n_2-1}{(n_2-1)(1-D)}$	$\frac{1+n_2}{1-D}$	$\frac{1+n_3+D}{1-D}$	$\frac{2n_2+n_3-1}{(1-D)(n_2-1)}$	$\frac{2+n_2+n_3(2-D)}{1-D}$

\* Note: S/D/C/CI+L= Quantity of Switches/Diodes/Capacitors/CIs + Inductors, LICR=Low Input Current Ripple.

**V. COMPARATIVE STUDY WITH SIMILAR TOPOLOGIES**

This section provides an extensive comparison between the suggested converter with available similar topologies in the literature. It is meant to identify the merits and demerits of the proposed topology, comparing with other available alternatives and help the engineers to select proper topology among many available varieties.

Table 1 shows the essential properties of the offered converter and comparable CI-based converters with an active switch that have recently been discussed in [12], [13], [14], [15], [16], [17], [18], [19], [20], and [21]. It includes voltage gain, normalized voltage stress (NVS) of the switch and diode, grounding approach, and component count. As shown in Table 1, the proposed topology achieves a considerably greater voltage gain and has less voltage stress on the power MOSFET than previous converters. Also, the smaller number of switches in the proposed converter than the converters provided in [14], [15], [19], and [20] makes the suggested converter easier to control. As a corollary, with appropriate design, the suggested topology can be able to use switch part with lower voltage ratings to obtain better efficiency. Another point that can be obtained from Table 1 is the fluctuation of the input current in the proposed converter versus the

compared converters. Unlike the converters described in [13], [15], [17], [19], [20], and [21], the suggested converter has a small input current ripple for wide load conditions.

Comparison of voltage gain from multiple high gain topology is shown in Fig. 8. In order to make a fair comparison between these converters, the number of secondary turns ( $N_2$ ) for two windings CI based converters was considered equal to 5 (equals the sum of the secondary and tertiary turn ratios in triple-winding converters). It can be found that with  $n_2 = 2.5$  and  $n_3 = 2.5$ , the suggested topology has a higher voltage conversion than the converters provided in [12], [13], [14], [15], [16], [17], [18], [19], [20], and [21] for all duty cycle values.

As shown in Fig. 9(a), the NVS of active MOSFET in the recommended topology is less than that of the topologies described in [12], [13], [14], [15], [16], [17], [18], [19], [20], and [21] for all duty cycle numbers. This feature causes the power MOSFET to be selected at a lower cost, which affects the overall cost of the converter.

Furthermore, Fig. 9(b) depicts the NVS of the output diode of the proposed topology and high step-up converters described in [12], [13], [14], [15], [16], [17], [18], [19], [20], and [21]. As it can be found from this Fig. 9(b), the NVS

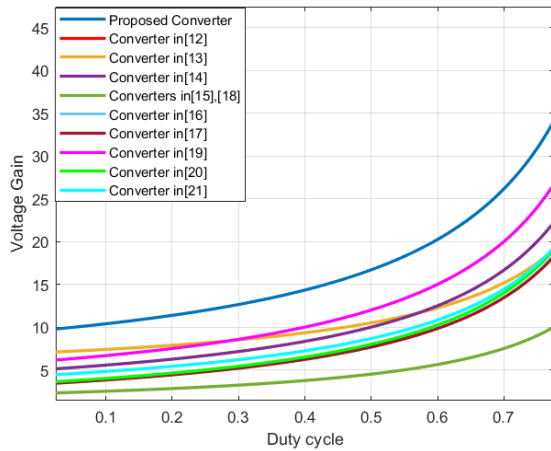


FIGURE 8. Comparison of voltage gain from multiple boost converters. ( $n_2 = 2.5$ , and  $n_3 = 2.5$  for three windings CIs and  $n_2 = 5$  for two windings CIs).

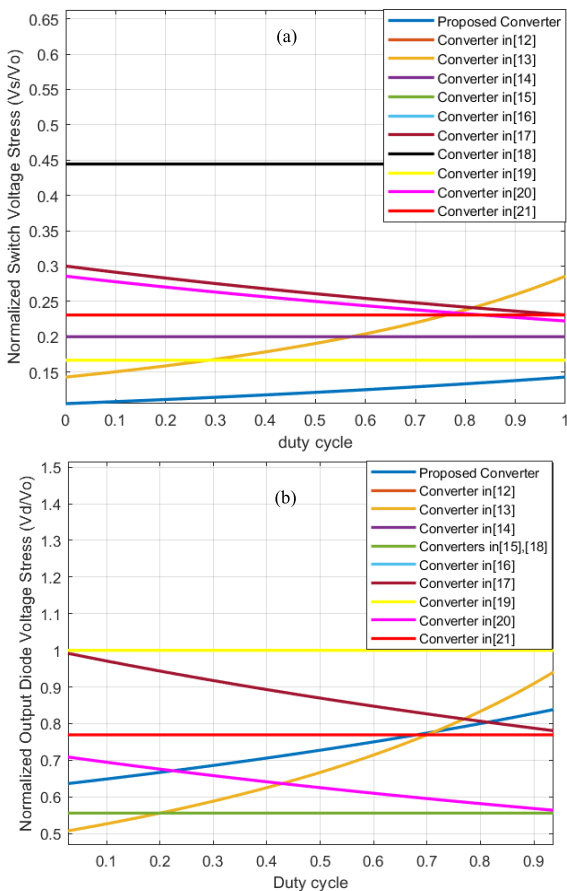


FIGURE 9. Features of high-gain topologies: (a) NVS of MOSFET, and (b) the output diode's NVS. ( $n_2 = 2.5$ , and  $n_3 = 2.5$  for three windings CIs and  $n_2 = 5$  for two windings CIs).

on output diode for suggested topology stays lower than output voltage for whole range of duty cycle. Furthermore, converters with lower voltage stress on their output diode

TABLE 2. Voltage ripple and the minimum value of the capacitors except resonance capacitors.

	$C_1$	$C_2$	$C_3$	$C_4$	$C_o$
Voltage ripple	2%	4%	4%	4%	0.1%
Minimum value	15.62 $\mu\text{F}$	3.47 $\mu\text{F}$	6.25 $\mu\text{F}$	6.25 $\mu\text{F}$	39.06 $\mu\text{F}$

TABLE 3. Current ripple and the minimum value of the inductors.

	$L_{in}$	$L_m$
Current ripple	15%	50%
The minimum value	121 $\mu\text{H}$	128 $\mu\text{H}$

than the suggested UHG topology often have weaker voltage boosting ability.

According to the comparative results, the suggested design has a much larger voltage gain than previous high step-up converters owing to the integration of three-winding CI, voltage lift capacitor ( $C_2$ ), and voltage multiplier unit. Furthermore, using a three-winding CI in the proposed scheme allows for easier voltage gain control and optimization of MOSFET and other semiconductor active component construction.

## VI. EXPERIMENTAL RESULTS

To evaluate the effectiveness and confirm the theoretical study of the suggested UHG converter, the outcomes of a 200 W built power circuit of the suggested converter are reported.

The peak to peak ripple of the output capacitor (and other capacitors in the converter circuit) is suggested to be kept under 5% [27]. In our work we have tried to design the converter by compromising the performance and cost factors. By substituting voltage ripple of Table 2 into (37) and assumed capacitors average current equal to  $I_o$ , the minimum size of capacitors are listed in the Table 2. (The ESR of the capacitors are ignored due to their small sizes):

The peak to peak ripple lower than 50% of the maximum inductor current gives a good compromise between the size of the inductor, that's proportional to weight and cost, and the RMS currents [27]. Similar to the calculation of capacitors, the inductors' size are obtained by assuming the acceptable current ripples as they are reported in Table 3:

The experimental model of the specified converter is seen in Fig. 10, and the characteristics for every element are listed in Table 4.

The outcomes of the topology working in CCM are shown in Fig. 11. Blue lines show voltage waveform and red lines represent current waveform in all of the figures.

Figure 11(a) depicts the voltage and current of diode  $D_1$ . This diode, as shown in the image, has a ZCS circumstance,



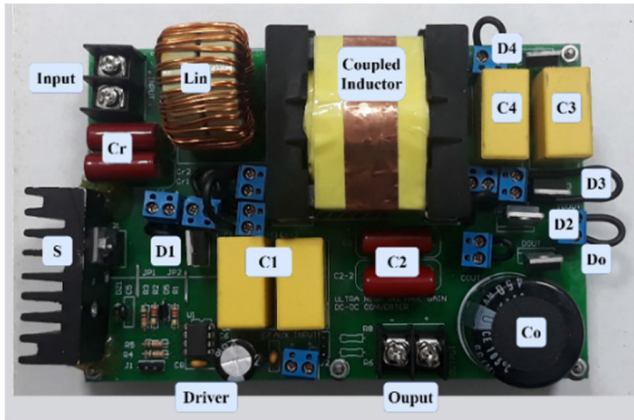


FIGURE 10. Experimental circuit of suggested UHG topology.

TABLE 4. Main parameters of experimental setup.

Parameters	Description/ Value
S	NCEP85T14, 3.6 mΩ on-resistance, $V_{DS}=85V, I_D=140A$
<b>Diodes</b>	
D <sub>1</sub> , D <sub>2</sub> , D <sub>3</sub> , D <sub>4</sub>	V30202C Schottky diode, $V_F=0.69 V$
D <sub>O</sub>	SBR40U300CT, $V_F=0.84 V$
<b>Magnetically Coupled Inductor (MCI)</b>	
	Turns ratio: ( $N_1: N_2: N_3=1: 2.5: 2.5$ )
	Core: ETD 49/25/16 ferrite core
	Magnetizing inductance: 140 μH
	Leakage inductance: 1.2 μH
<b>Inductors</b>	
L <sub>in</sub>	100 μH
	Core: double T131-52 iron powder core
<b>Capacitors</b>	
C <sub>1</sub>	2*8.2 μF, 63 V
C <sub>2</sub>	2*2.2 μF, 400 V
C <sub>3</sub> , C <sub>4</sub>	8.2 μF, 63 V
C <sub>O</sub>	330 μF, 450 V
C <sub>r</sub>	2*2.2 μF, 400 V
Switching Frequency	50 kHz
Output Power	200 W
Input Voltage	17-20 V
Output Voltage	320 V
Nominal Gain	16

and its voltage waveform verifies the study provided in (18). As it can be found from Figure 11(a) after the current of diode D<sub>1</sub> reaches a maximum, its current decreases slowly. So soft switching occurs when the current reaches zero (According to Mode 5 and Mode 6 in section II).

The voltage and current waveforms of diode D<sub>2</sub> are depicted in Fig. 11(b). Because the current of this diode varies with a tiny slope (Not suddenly with a steep slope) when it is turned on and off, it has a ZCS characteristic both when it is turned on and when it is turned off.

The waveforms of diode D<sub>3</sub> are shown in Fig. 11(c). This diode, like diode D<sub>2</sub>, has a ZCS behavior in both turning on and off. This diode’s voltage waveform confirms the theoretical computations given in (20). As can be found from this figure After the voltage applied to the diode is zero, the current starts to increase with a low slope. Therefore,

the overlap between voltage and current will be very low when the state of diode is changed (According to Mode 3 in section II).

Fig. 11(d) is related to the output diode D<sub>O</sub>. As it can be found, this diode is turned off in ZCS situation which will reduce the reverse recovery losses significantly. It can decrease the total cost of the system since its voltage stress is smaller than the output voltage.

The voltage and current of input inductor L<sub>in</sub> are shown in Fig. 11(e). The continuation of the input current is a crucial aspect in several uses, particularly the utilization of solar panels. The average input current in Fig. 11(e) is 10 A, with a ripple of 150 mA. The voltages and currents in the CI primary and secondary windings are shown in Figs. 11(f) and 11(g), accordingly. The maximum voltage and current of L<sub>N1</sub> are 35V, 12A respectively. The maximum voltage and current of L<sub>N2</sub> are 100 V and 3A respectively.

The drain-to-source voltage and drain current of the MOSFET are shown in Fig. 11(h). The zoomed-in picture shows that this switch has a smooth switching action and that the switching losses are so low that they can be disregarded (According to explanations of Mode 1 in section II). If the rated current of the desired switch is less than that of the converter, or in order to increase the power of the proposed converter, several MOSFETs can be paralleled and increase the power of the converter.

The nominal and experimental prototype output voltages are shown in Fig. 12 to examine the correctness of the derived ideal voltage gain and compare it to actual voltage gain. Since one of the main advantages of this converter is to achieve high voltage gain in low duty cycle values, in this figure, the duty cycle is not considered higher than 0.6. Also, when duty cycle is high, the efficiency drops from our desired level and the conductive losses of the switch increase.

The output voltage, input current and their ripples are shown in Figure 13. As it can be found from this figure, the input current and output voltage ripple of suggested converter is very low. Furthermore, these figures meet the requirements set in Tables 2, 3. This converter is suitable for applications that require a low current ripple on the input side such as fuel cell and PV applications.

The waveform of the output voltage of the proposed converter with transient step load change is shown in Figure 14. As it can be seen, the proposed converter has an appropriate transient response when load is changed from %100 to %50 of its nominal power. In this figure the voltage overshoot is about 30V and the response time is around 250 ms. Due to the presence of only one active switch in the proposed converter, the closed loop state can be implemented with analog or digital circuits.

#### A. EFFICIENCY ANALYSIS

According to Table 4, in order to accurately evaluate the performance of the converter, it’s better to analyze the converter losses by calculating the converter efficiency at 200 Watts. In general, the converter losses can be divided into 4 groups:

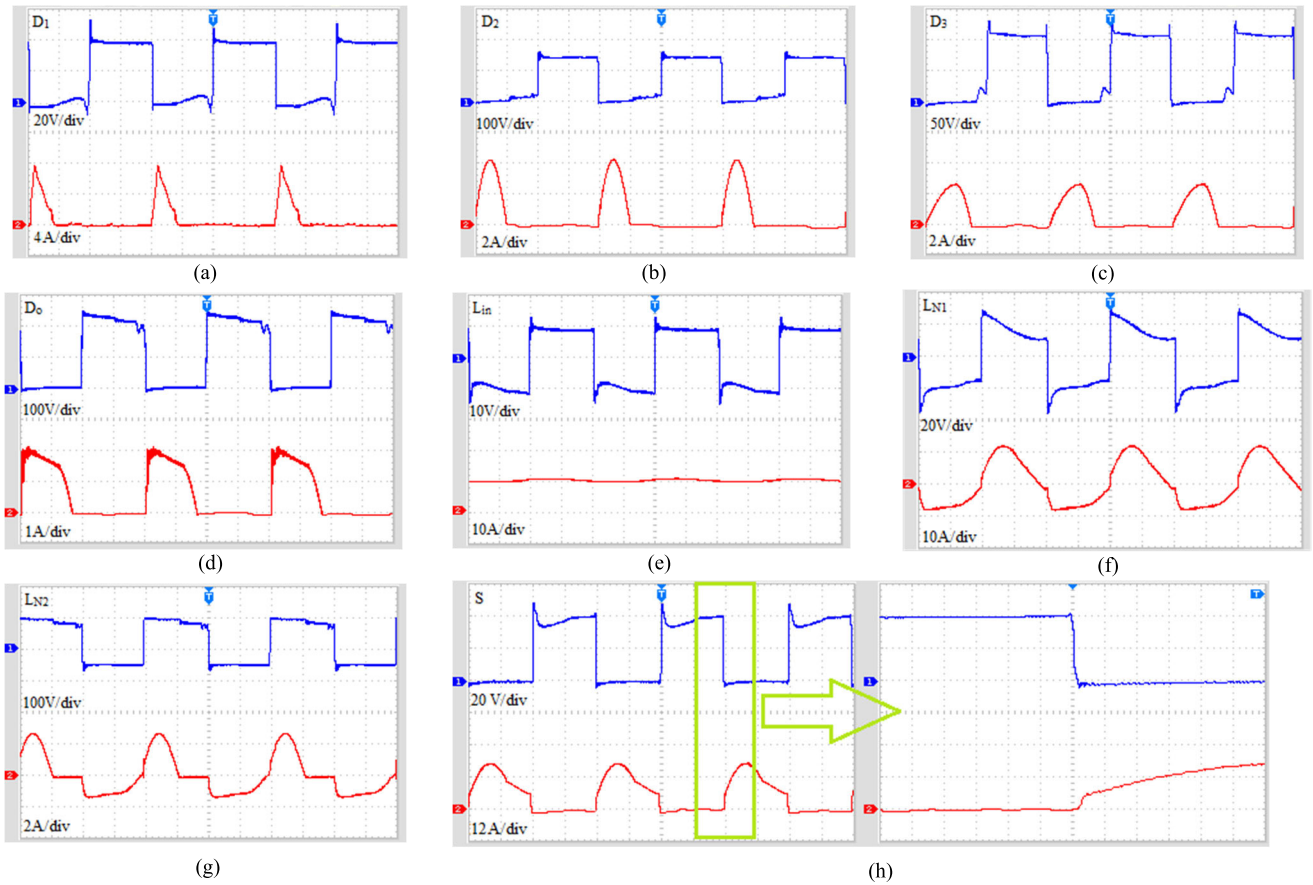


**FIGURE 11.** Experimental results of UHG Converter. Voltage and current in: (a) D1 (b) D2 (c) D3 (d) Do (e) Lin (f) LN1 (g) LN2 (h) Active switch, time:  $5 \mu\text{s}/\text{div}$ .

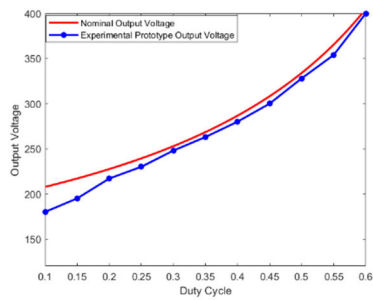


**FIGURE 12.** Nominal and experimental prototype output voltages.

1) SWITCH LOSSES

Switch losses are divided into two categories: switching losses and conduction losses. Because of the soft switching of the topology at the moment when the switch is turned on, its switching losses only include losses during turning off. To calculate conduction losses and switching losses the following equation is needed:

$$P_{loss(turn\ OFF)} = \left( \frac{1}{2} * V_{ds} * I_{ds} * t_{turn-off\ fall\ time} \right) * f_s = 0.34 \tag{41}$$

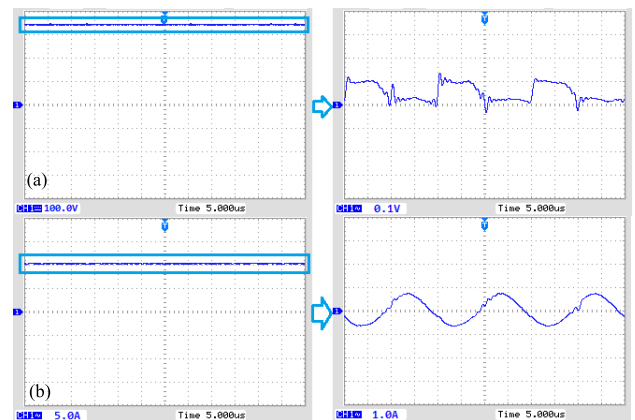


**FIGURE 13.** (a) Voltage ripple of output capacitor (b) Current ripple of input inductor  $L_{in}$ .

where  $t_{turn-off}$  fall time of the MOSFET in our experimental set-up is about 20 nano-seconds in  $I_{DS} = 17\text{A}$ .

$$P_{loss(conduction)} = R_{ds(on)} * I_{ds(RMS)}^2 = 1.04\text{ W} \tag{42}$$

$$P_{loss(switch)} = P_{loss(turnOFF)} + P_{loss(conductionswitch)} = 1.38\text{ W} \tag{43}$$

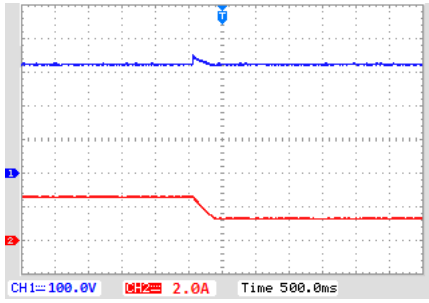


FIGURE 14. Converter response when output load changes from %100 to %50 (blue curve: output voltage, red curve: output current).

2) DIODE LOSSES

In the case of diodes, the ohmic losses of the diodes and the reverse recovery loss of the diodes in this topology are ignorable and the main losses of the diodes are related to the voltage drop of the diodes in its average currents (conduction losses). For this reason, the following equation can be considered:

$$P_{loss(diode)} = V_{forward\ diode} \times I_{D(average)} = 2.25\ W \quad (44)$$

3) CAPACITOR OHMIC LOSS

In order to calculate the internal resistance loss of capacitors, the following equation can be considered:

$$P_{loss(capacitor)} = ESR \times I_{COUT(RMS)}^2 = 0.059\ W \quad (45)$$

Only the output capacitor is considered because the rest of capacitors have a small ESR due to their material (MKT and Polyester).  $I_{cout(rms)}$  is RMS current of output capacitor and it is approximately to  $I_O$ .

4) MAGNETIC LOSSES

According to T131-52 iron powder core datasheet the core loss of input inductor is considered  $125\ mW/cm^3$  and the volume of each inductor is  $13.68\ cm^3$ . The same as input inductors, according to ETD49/25/16 datasheet the core loss of CI is considered  $139\ mW/cm^3$  and the volume of each inductor is  $24.3\ mW/cm^3$ . The ohmic loss is equal and due to the large number of primary wire (they are wrapped in litz wire) the ohmic loss is negligible. Therefore, to calculate the core loss we can consider:

$$P_{loss(core)} = 3.38 + 1.7 = 5.08\ W \quad (46)$$

According to the equation of losses in previous sections, the efficiency of topology can be calculated as follows:

$$\eta = \frac{P_O}{P_O + P_{loss}} = \frac{200}{200 + 8.77} = 95.80\% \quad (47)$$

The total losses shown by (41)-(47) is illustrated as a pie chart in Fig. 15 for the implemented converter, where  $V_{in}$  is 18V and the output load is 200 W. This pie plots show that switch losses is low due to its low voltage ripple.

Fig. 16 depicts an efficiency comparison between the suggested topology and the converters based on CIs described in

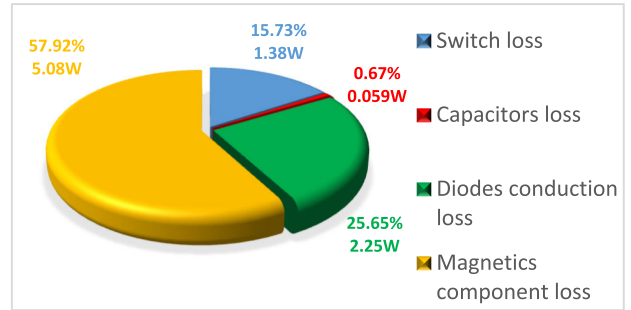


FIGURE 15. Comparison of voltage gain from multiple boost converters. ( $N_2 = 2.5$ , and  $N_3 = 2.5$ ).

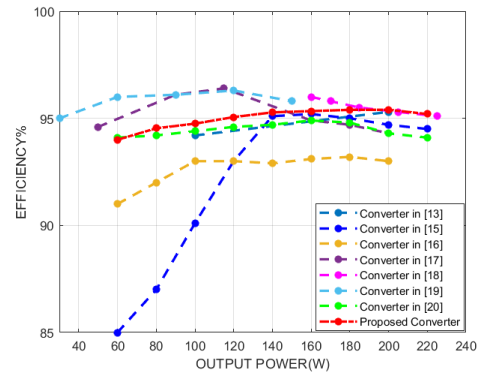


FIGURE 16. Comparison of efficiency in different loads.

[13], [15], [16], [17], [18], [19], and [20] for different loads levels. The main reason for improving the efficiency is the ability to use the MOSFET with a small  $R_{ds}$  due to lower voltage stress on the switch and the ZCS operation of the main switch in the on state. Also, alleviating the reverse diode recovery issue and ZCS operation of diodes in this topology help to improve the overall efficiency of the converter.

VII. CONCLUSION

This work presents an ultra-high voltage gain (UHG) DC-DC structure depending on three windings coupled inductor (CI) and voltage multiplier cell (VMC). The crucial benefits of the proposed configuration are:

- ultra-high gain in a significant low turn ratio of CI and suitable zone of duty cycles, recycled energy of inductor. Comparison with similar topologies showed this superiority.
- Efficiency improvements due to soft switching process for main switch and other diodes. Comparison with similar converters showed appropriate converter efficiency.
- Low normalized voltage stress (NVS) on MOSFETs and other electronic components. The investigation of voltage stresses on components and experimental results confirmed this superiority.
- Low input current ripple, which causes less stress on the input source than the high current ripple converters. The experimental results verified this capability.



The principle of operation of the converter and its steady-state assessment under CCM situations have been comprehensively described.

Furthermore, the proposed UHG converter has two intrinsic characteristics that make it suited for use as a solar panel side DC-DC converter in Photovoltaic system. First, the input current is continuous and has a very small ripple. The second characteristic is its common ground, that can avoid common mode leakage current. Input current continuous simplifies the installation of maximum power point tracking (MPPT) controls, and the common ground characteristic can reduce the requirement for complicated leakage current control in PV system applications [25], [26].

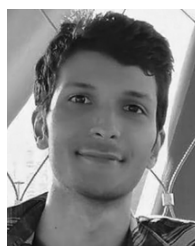
Some other practical applications of the suggested converter are as follows:

- DC microgrid application.
- LED lightning.
- Automobile headlight (HID).
- Robotics.

The closed loop analysis and transient response of the suggested converter in different conditions can be studied in more detail in the future works.

## REFERENCES

- [1] R. Faranda, H. Hafezi, S. Leva, M. Mussetta, and E. Ogliari, "The optimum PV plant for a given solar DC/AC converter," *Energies*, vol. 8, no. 6, pp. 4853–4870, May 2015.
- [2] M. S. Bhaskar, V. K. Ramachandaramurthy, S. Padmanaban, F. Blaabjerg, D. M. Ionel, M. Mitolo, and D. Almakhlis, "Survey of DC-DC non-isolated topologies for unidirectional power flow in fuel cell vehicles," *IEEE Access*, vol. 8, pp. 178130–178166, 2020.
- [3] O. Cornea, D. Hulea, N. Muntean, and G.-D. Andreescu, "Step-down switched-inductor hybrid DC-DC converter for small power wind energy conversion systems with hybrid storage," *IEEE Access*, vol. 8, pp. 136092–136107, 2020.
- [4] A. Affam, Y. M. Buswig, A.-K.-B. H. Othman, N. B. Julai, and O. Qays, "A review of multiple input DC-DC converter topologies linked with hybrid electric vehicles and renewable energy systems," *Renew. Sustain. Energy Rev.*, vol. 135, Jan. 2021, Art. no. 110186.
- [5] C. Parthasarathy, H. Hafezi, H. Laaksonen, and K. Kauhaniemi, "Modelling and simulation of hybrid PV & BES systems as flexible resources in smartgrids—Sundom smart grid case," in *Proc. IEEE Milan PowerTech*, 2019, pp. 1–6.
- [6] S. Talebi, E. Adib, and M. Delshad, "A high-gain interleaved DC-DC converter with passive clamp circuit and low current ripple," *Iranian J. Sci. Technol., Trans. Electr. Eng.*, vol. 45, no. 1, pp. 141–153, Mar. 2021.
- [7] S. Saravanan and N. R. Babu, "Analysis and implementation of high step-up DC-DC converter for PV based grid application," *Appl. Energy*, vol. 190, pp. 64–72, Mar. 2017.
- [8] B.-R. Lin and Y.-C. Liu, "Implementation of a wide input voltage resonant converter with voltage doubler rectifier topology," *Electronics*, vol. 9, no. 11, p. 1931, Nov. 2020.
- [9] H. Ardi, A. Ajami, and M. Sabahi, "A novel high step-up DC-DC converter with continuous input current integrating coupled inductor for renewable energy applications," *IEEE Trans. Ind. Electron.*, vol. 65, no. 2, pp. 1306–1315, Feb. 2018.
- [10] H. Liu, H. Hu, H. Wu, Y. Xing, and I. Batarseh, "Overview of high-step-up coupled-inductor boost converters," *IEEE J. Emerg. Sel. Topics Power Electron.*, vol. 4, no. 2, pp. 689–704, Jun. 2016.
- [11] X. Fan, H. Sun, Z. Yuan, C. Li, R. Shi, and N. Ghadimi, "High voltage gain DC/DC converter using coupled inductor and VM techniques," *IEEE Access*, vol. 8, pp. 131975–131987, 2020.
- [12] R. Xian, X. Liu, F. Li, Y. Yao, N. Geng, J. Yang, L. Liu, Y. Sun, Z. Yue, C. Cui, and Y. Yu, "High step-up DC-DC converter with three-winding-coupled-inductor and output capacitor in series for clean energy," *IET Power Electron.*, vol. 12, no. 5, pp. 1087–1093, 2019.
- [13] K.-C. Tseng, J.-T. Lin, and C.-C. Huang, "High step-up converter with three-winding coupled inductor for fuel cell energy source applications," *IEEE Trans. Power Electron.*, vol. 30, no. 2, pp. 574–581, Feb. 2015.
- [14] A. Kumar and P. Sensarma, "Ripple-free input current high voltage gain DC-DC converters with coupled inductors," *IEEE Trans. Power Electron.*, vol. 34, no. 4, pp. 3418–3428, Apr. 2019.
- [15] H. Liu, L. Wang, Y. Ji, and F. Li, "A novel reversal coupled inductor high-conversion-ratio bidirectional DC-DC converter," *IEEE Trans. Power Electron.*, vol. 33, no. 6, pp. 4968–4979, Jun. 2018.
- [16] J. Yao, A. Abramovitz, and K. M. Smedley, "Analysis and design of charge pump-assisted high step-up tapped inductor SEPIC converter with an 'inductorless' regenerative snubber," *IEEE Trans. Power Electron.*, vol. 30, no. 10, pp. 5565–5580, Oct. 2015.
- [17] M. Mahmoudi, A. Ajami, and E. Babaei, "A single switch high step-up DC-DC converter with three winding coupled inductor," *Int. Trans. Electr. Energy Syst.*, vol. 29, no. 1, p. e2668, Jan. 2019.
- [18] S. Pourjafar, H. Shayeghi, H. M. Kojabadi, M. Maalandish, and F. Sedaghati, "A coupled inductor based high voltage gain DC-DC converter using interleaved voltage multiplier cells," *Iranian J. Electr. Electron. Eng.*, vol. 16, no. 1, pp. 1–12, 2020.
- [19] R. Faraji and H. Farzanehfard, "Soft-switched nonisolated high step-up three-port DC-DC converter for hybrid energy systems," *IEEE Trans. Power Electron.*, vol. 33, no. 12, pp. 10101–10111, Dec. 2018.
- [20] Y. Tang, D. Fu, J. Kan, and T. Wang, "Dual switches DC/DC converter with three-winding-coupled inductor and charge pump," *IEEE Trans. Power Electron.*, vol. 31, no. 1, pp. 461–469, Jan. 2016.
- [21] F. Li, Y. Yao, Z. Wang, and H. Liu, "Coupled-inductor-inverse high step-up converter," *IET Power Electron.*, vol. 11, no. 5, pp. 902–911, 2018.
- [22] M. E. Azizkandi, F. Sedaghati, H. Shayeghi, and F. Blaabjerg, "A high voltage gain DC-DC converter based on three winding coupled inductor and voltage multiplier cell," *IEEE Trans. Power Electron.*, vol. 35, no. 5, pp. 4558–4567, May 2020.
- [23] M. Forouzesh, K. Yari, A. Baghrarian, and S. Hasanpour, "Single-switch high step-up converter based on coupled inductor and switched capacitor techniques with quasi-resonant operation," *IET Power Electron.*, vol. 10, no. 2, pp. 240–250, Feb. 2017.
- [24] M. Farsijani, S. Abbasian, H. Hafezi, M. Tavakolibina, and K. Abbaszadeh, "A single-switch ultra-high gain DC-DC converter with low input current ripple and ZCS," in *Proc. Int. Conf. Smart Energy Syst. Technol. (SEST)*, Sep. 2021, pp. 1–6, doi: 10.1109/SEST50973.2021.9543416.
- [25] A. Sabry, Z. M. Mohammed, F. H. Nordin, N. H. N. Ali, and A. S. Al-Ogaili, "Single-phase grid-tied transformerless inverter of zero leakage current for PV system," *IEEE Access*, vol. 8, pp. 4361–4371, 2020.
- [26] Z. Ahmad and S. N. Singh, "Single phase transformerless inverter topology with reduced leakage current for grid connected photovoltaic system," *Electr. Power Syst. Res.*, vol. 154, pp. 193–203, Jan. 2018.
- [27] R. W. Erickson and D. Maksimović, *Fundamentals of Power Electronics*. Berlin, Germany: Springer, 2020.
- [28] S. Abbasian, M. Farsijani, M. T. Bina, and A. Shahirinia, "A non-isolated common-ground high step-up soft switching DC-DC converter with single active switch," *IEEE Trans. Ind. Electron.*, early access, Aug. 17, 2022, doi: 10.1109/TIE.2022.3198262.
- [29] J. Y. Lee, Y. S. Jeong, and B. M. Han, "An isolated DC/DC converter using high-frequency unregulated LLC resonant converter for fuel cell applications," *IEEE Trans. Ind. Electron.*, vol. 58, no. 7, pp. 2926–2934, Jul. 2011.



**MOHAMMAD FARSIJANI** (Member, IEEE) was born in Tehran, Iran, in 1996. He received the M.Sc. degree from the K. N. Toosi University of Technology (KNTU), Tehran, in 2021. He is currently working with the KNTU Laboratory. He is one of the Research and Development Expert Team at JDEVS Company. His research interests include multi-level inverters, high-gain dc-dc converter, control methods in UPS application, and common-mode noise reduction in power electronics systems. He is a Reviewer of the IEEE TRANSACTIONS ON POWER ELECTRONICS and IEEE ACCESS journals.



**SOHRAB ABBASIAN** (Member, IEEE) was born in Babol, Iran, in 1995. He received the B.Sc. degree from the Noshirvani University of Technology, Babol, in 2018. He is currently pursuing the master's degree with the K. N. Toosi University of Technology (KNTU), Tehran, Iran. His research interests include high-gain dc–dc converters and soft-switching techniques for dc–dc converters.



**HOSSEIN HAFEZI** (Senior Member, IEEE) received the B.Sc. degree from the K. N. Toosi University of Technology, Tehran, Iran, in 2008, the M.Sc. degree from Dokuz Eylul University, Izmir, Turkey, in 2013, and the Ph.D. degree from the Energy Department, Politecnico di Milano, Milan, Italy, in 2017, all in electrical engineering. His employment experience includes working as a Postdoctoral Research Fellow at the Energy Department, Politecnico di Milano, and as an

Assistant Professor at the School of Technology and Innovations, Electrical Engineering, University of Vaasa, Finland. Since September 2020, he has been an University Lecturer with the Faculty of Information Technology and Communication Sciences, Tampere University. His research interests include power electronics converters design and control, power electronics and its applications in power quality improvement and smart grids systems, renewable energies integration into modern and smart grid systems and their effects on power quality and system operation, dc and hybrid dc–ac low-voltage distribution systems, microgrid systems, and electric power system studies.



**MOHAMMAD TAVAKOLI BINA** (Senior Member, IEEE) received the B.Sc. degree in power electronics and power system utility applications from the University of Tehran, Tehran, Iran, in 1988, the M.Sc. degree in power electronics and power system utility applications from the University of Ferdowsi, Mashhad, Iran, in 1991, and the Ph.D. degree from the University of Surrey, Guildford, U.K., in 2001. From 1992 to 1997, he was a Lecturer at the K. N. Toosi University of Technology, Tehran, where he was involved in power systems. He joined the Faculty of Electrical and Computer Engineering, K. N. Toosi University of Technology, in 2001, where he is currently a Professor in power electronics and electrical engineering, and involved in lecturing and conducting research in the area of power electronics and utility applications.



**KARIM ABBASZADEH** received the B.S. degree in communication engineering from the Khaled Nasir Toosi University of Technology, Tehran, Iran, in 1991, and the M.S. and Ph.D. degrees in electrical engineering from the Amir Kabir University of Technology, Tehran, in 1997 and 2000, respectively. From 2001 to 2003, he was a Research Assistant at the Department of Electrical Engineering, Texas A&M University, College Station, TX, USA. He is currently a Professor with the Department of Electrical Engineering, Khajeh Nasir Toosi University of Technology. He is actively involved in presenting short courses and consulting in his area of expertise to various industries. He is the author of more than 50 published journal articles. His research interests include power electronic and dc–dc and dc–ac converters, electric machinery, variable-speed drives, and propulsion applications.

• • •